ELSEVIER

Polymer 42 (2001) 7161–7170

polymer

www.elsevier.nl/locate/polymer

In situ study of structure development during continuous hot-drawing of poly(trimethylene terephthalate) fibers by simultaneous synchrotron small- and wide-angle X-ray scattering

Jing Wu[a], Jerold M. Schultz[a,*], Joshua M. Samon[a], Adriano B. Pangelinan[b], Hoe H. Chuah[b]

[a]*Department of Chemical Engineering, University of Delaware, Newark, DE 19716, USA*
[b]*Westhollow Technology Center, Shell Chemical Company, Houston, TX 77251, USA*

Received 30 September 2000; received in revised form 25 November 2000; accepted 2 December 2000

Abstract

Off-line small- and wide-angle X-ray scattering and optical birefringence measurements on partially oriented yarns (POY) of poly(trimethylene terephthalate) prepared at different take-up speeds suggest the formation of a rigid amorphous phase for intermediate take-up speed POY. Simultaneous synchrotron small-angle X-ray scattering (SAXS) and wide-angle X-ray diffraction (WAXD) techniques were utilized to perform an in situ study of structure development of these POY during continuous hot-drawing. From SAXS patterns, it is suggested that a lamellar stacking arises at temperature above 100°C during drawing. A model of lateral growth of crystallites with extended chains as nucleation sites is suggested. The microfibril length and long period of the lamellar stacking depend upon the preparation take-up speeds of POY and draw ratio. From WAXD patterns, it is observed that crystallinity developed above 100°C with draw ratio 1:1 is temperature controlled. Both orientation and unit cell dimensions were extracted from WAXD patterns. At 100°C, while orientation increases with draw ratio, the unit cell dimensions, especially the dimension of the *c*-axis, and the crystallinity depend on both draw ratio and take-up speeds. This dependence can be explained by a transformation process coupled by defect creation/transport and crystallization.

Keywords: Poly(trimethylene terephthalate); Fibers; Continuous hot-drawing

1. Introduction

Poly(trimethylene terephthalate) (PTT), also known as 3GT, belongs to the polyester family, among which both poly(ethylene terephthalate) (PET) and poly(butylene terephthalate) (PBT) are important members. Of these, PET and PBT have been studied thoroughly during the last decades. PTT, on the other hand, is of recent interest because of Shell's discovery of a low-cost monomer process and because of its excellent fiber properties.

The crystal structure of PTT was determined by Desborough and Hall et al. [1], Poulin-Dandurand et al. [2] and by Tadokoro [3]. All these researchers agree that the unit cell of PTT is triclinic and the crystal space group is $P\bar{1}$. Each cell contains two monomers of one polymer chain. The molecular configuration consists of rigid planar terephthaloyl residues alternating with a more flexible trimethylene sequence. The $O–CH_2–CH_2–CH_2–O$ segment of the chain has a near *trans–gauche–gauche–trans* conformation. The unit cell parameters determined by the three groups of researchers are close. According to Poulin-Dandurand [2], the unit cell of PTT is triclinic, with $a = 4.637$ Å, $b = 6.226$ Å, $c = 18.64$ Å, $\alpha = 98.4°$, $\beta = 93.0°$ and $\gamma = 111.5°$. However, there are differences in specific d-spacing values. The reported crystal structures of PTT were reviewed by Hall [4].

Crystal deformation of PTT fiber was studied by Jakeways and Ward [5] and the corresponding mechanical properties were reported by Ward in a separate publication [6]. These studies showed that PTT had an elastic unit cell, which responded immediately to the applied stress. The polymer chains deform like a spring along the fiber axis with application of stress and there is substantial recovery when stress is removed. PTT's excellent stress recovery property is similar to that of nylon and this makes PTT an excellent candidate for textile applications.

In commercial processing, PTT is first spun into a partially oriented yarn (POY), then the POY is hot-drawn to a certain draw ratio, followed by subsequent

* Corresponding author. Tel.: +1-302-831-2543; fax: +1-302-831-1048.
E-mail address: schultz@che.udel.edu (J.M. Schultz).

0032-3861/01/$ - see front matter
PII: S0032-3861(01)00045-3

heat treatment such as texturing and twisting. The tandem processes of spinning and hot-drawing are used to establish a microstructure consistent with good thermal stability, bulk and strength, which can be further modified by texturing and twisting. 'Microstructure' here refers to molecular structure and conformation, crystallite sizes and shapes, and arrangement of crystalline and noncrystalline regions.

Hot-drawing and subsequent heat treatment are dynamic in nature. The microstructure changes continuously during processing. There have been several studies of on-line characterization of structure development of fibers during hot-drawing using laboratory X-ray generators [7–9]. However, these experiments suffered difficulties such as long exposure time and low signal to noise ratio due to the relatively low X-ray intensity produced by in-house generators. With increasing accessibility of synchrotron X-ray radiation, the above-mentioned problems can be overcome. Hsiao et al. [10] demonstrated the integration of a drawing apparatus with a synchrotron beamline and studied the drawing behavior of Nylon 66.

To our knowledge, structure development of PTT fibers during hot-drawing has not been addressed. On the other hand, there is extensive research on this subject for PET. It is useful to review these studies in order to set the context of the present one.

Studies of crystallization kinetics of PET by Smith and Steward [11], Alfonso et al. [12] and Althen and Zachmann [13] suggested that crystallization rate increases with orientation, which is in accord with theories [14–17] developed for oriented polymer crystallization. These theories generally predict that nucleation and growth rates increase with orientation.

Other studies characterized PET fibers after heat-treatment. Pioneer research by Dismore and Statton [18,19] and by Dumbleton [20] suggested a folded-chain morphology for drawn PET yarns annealed under unconstrained conditions. Liska [21] studied PET as-spun fibers and corresponding fibers subject to hot-drawing. The orientation of crystallites deduced from WAXD patterns increased with draw ratio and correlated very well with the morphology suggested by SAXS results, which suggested the modified Hess–Kiessig model proposed by Bonart [22]. Fischer and Fakirov's SAXS results [23] suggested a microstructure of mosaic blocks with folded chains. Gupte et al. [24] characterized PET fibers annealed under different temperatures and time. They proposed a two-stage transformation model for crystallization and morphology formation. A lamellar tilt mechanism was also suggested.

The present work is aimed at understanding of the in situ structure development of PTT POY during continuous hot-drawing by using simultaneous synchrotron small-angle X-ray scattering (SAXS) and wide-angle X-ray diffraction (WAXD) techniques.

2. Experimental

The PTT fibers were provided by Shell Chemical Company. They are commercially known as Corterra™. The pellets producing the fiber have an intrinsic viscosity of 0.92 and the corresponding M_w is 48,700 with an M_w to M_n ratio of 2. The fibers consisted of POY prepared at take-up speeds of 980, 1470, 2040, 2550, 3050, 3545 and 4185 m/min. Synchrotron X-ray measurement was carried out at the Beamline X3A2 of the National Synchrotron Light Source, Brookhaven National Laboratory ($\lambda = 1.275$ Å, beam diameter = 300 μm). A double-multilayer (silicon/tungsten) monochromator was used to monochromatize the white synchrotron X-ray beam. The resulting beam has an energy resolution of 1.5%. A continuous drawing apparatus (constructed by Hills Inc., W. Melbourne, Florida) was used to perform continuous hot drawing of PTT POY and it is sketched in Fig. 1. The speeds of the upper roll, i.e. the feed-roll, and the lower roll, also known as the draw-roll, can be controlled independently. The draw-roll usually operates at a higher speed then the feed-roll. A draw ratio is defined as the ratio between the speeds of the draw- and the feed-roll. A hot pin was utilized to heat the fiber to temperatures of 70, 100 or 130°C. At a specific temperature, the fibers were drawn with varying draw ratio ranging from 1:1 to 3:1. For this study, the feed speed was kept at 5 m/min, while the draw speed was continuously adjusted in order to achieve the desired draw ratio. For each type of POY at a certain temperature, effort was made to achieve the maximum draw ratio possible. Care was taken to ensure that the fibers were vertical to the primary X-ray beam. Detailed experimental conditions are shown in Table 1. When the drawing line was stable, 2D WAXD and SAXS scattering patterns were recorded simultaneously by two Fuji™ HR-V imaging plates. The sample to detector distance for WAXD and SAXS are 90 and 1138 mm, respectively. The imaging plates were digitized by a Fuji™ BAS 2000 scanner with a

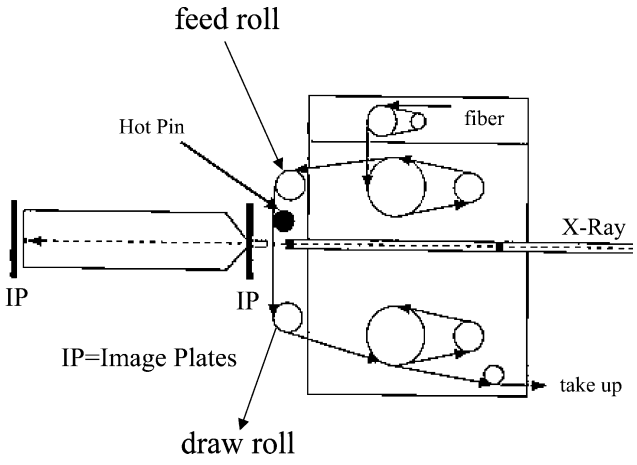

Fig. 1. Experimental setup for simultaneous measurement of WAXD and SAXS during continuous hot drawing. In the figure, IP is an abbreviation for imaging plate.

Table 1
Drawing conditions for PTT POY (Entries in the table: Maximum draw ratio. Draw ratio starts from 1:1, with an increment step of 0.1 or 0.2)

Take-up speed (m/min)	980	1470	2040	2550	3050	3545	4185
$T = 70$°C	3:1	–[a]	–[a]	2.5:1	–[a]	–[a]	1.7:1
$T = 100$°C	3:1	–[a]	–[a]	2:1	–[a]	–[a]	1.5:1
$T = 130$°C	1:1	1.2:1	1.5:1	1.5:1	1.2:1	1.2:1	1:1

[a] Scattering not performed.

resolution of 100 μm for both WAXD and SAXS patterns. A central hole of 2.5 cm diameter was cut on each WAXD imaging plate to allow passage and registration of the SAXS signal. A typical collection time for WAXD patterns was 2 min and for SAXS patterns 4 min. The recorded WAXD and SAXS patterns or their corresponding one-dimensional (1D) extracted profiles were subject to incident beam intensity, background and scattering volume corrections.

The SAXS and WAXD patterns were also collected from all POY at room temperature without drawing, with the fiber axis perpendicular to the X-ray beam.

3. Data analysis

3.1. Unit cell parameters determined from WAXD

Sixteen reflections can be identified on a 2D WAXD pattern. A typical pattern is shown in Fig. 2. Indices for all peaks were assigned as well. Out of these 16 reflections, thirteen were used the refine the unit cell parameters. For overlapping reflections equal weight fractions were assigned for each reflection during regression. The 1.5% energy resolution of the incident beam gives rise to a relative error of 1.5% for the d-spacing measurement. The standard deviations for the calculated unit cell parameters are all less than 2%.

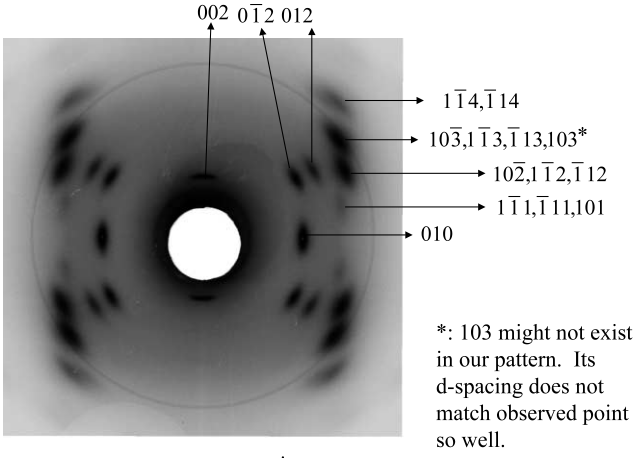

Fig. 2. A typical 2D WAXD pattern with indexing of individual peaks.

3.2. Overall crystallinity index from WAXD

In order to further analyze 2D WAXD patterns such as the one shown in Fig. 2 were analyzed following the procedure given previously [25]. Briefly, the procedure is as follows. For all diffraction angles in the range 2θ, range 8.2–41.6°, the diffracted intensity is integrated azimuthally from 0 to 360°, followed by normalization by the number of pixels contributing to the integration and deconvolution into crystalline diffraction peaks and an amorphous halo. The overall crystallinity index is then taken as [26] $A_c/A_c + A_a$, where A_c and A_a are the sum of areas under the crystalline and amorphous peaks, respectively. The random errors originating from the peak deconvolution are obtained by calculating the percentage of the residuals after the peak deconvolution process. Systematic errors resulting from the Gaussian peak shape assumption in the deconvolution should be similar in all patterns.

3.3. Orientation of the crystallites from WAXD

The Hermans crystal orientation factor [27–29] was obtained from the azimuthal profile of the (010) reflection, using Wilchinsky's method [30,31]. The procedure used was given previously [25].

3.4. SAXS analysis to calculate the dimensions of lamellar morphology

Typical 2D SAXS patterns from semicrystalline polymers exhibit two lobes along the meridian and an equatorial streak. This suggests the existence of narrow stacks of lamellae [32], i.e. stacks of alternating crystalline and non-crystalline layers. This periodic repeat of crystalline and non-crystalline layers gives rise to the two-lobe scattering pattern, while the narrow stacks of lamellae as a whole, i.e. microfibrils, gives rise to the equatorial streak. During our experiment, SAXS patterns having this feature were observed under most conditions. Fig. 4 of Ref. 25 shows a typical 2D SAXS pattern bearing this feature.

3.4.1. Long period

The characteristic longitudinal dimension of the lamellar stack, i.e. long period, was extracted using correlation function ($\gamma(r)$) analysis [33].

(1) A projection operation was first applied to obtain the integrated intensity on the meridian ($I_1(q_3)$) using the following formalism:

$$I_1(q_3) = \int_0^\infty I(q_{12}, q_3) q_{12}\, \mathrm{d}q_{12}, \tag{1}$$

where $q = 4\pi \sin\theta/\lambda$ is the scattering vector. The subscript 3 represents the meridinal direction and the subscript 12 represents equatorial directions. In order to obtain scattering intensity profiles solely from the lamellar structure, the intensity in a rectangular region, whose height just covers the beam stop, was set to zero to exclude scattering from the

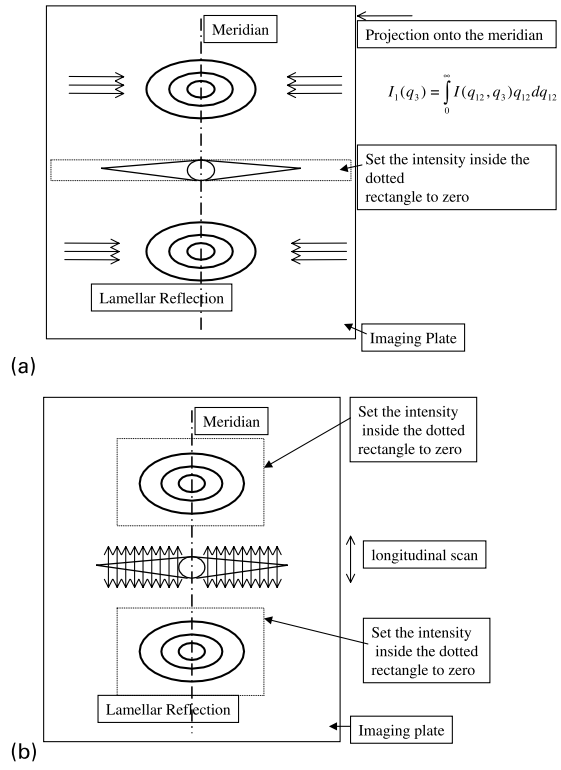

Fig. 3. Diagram for SAXS pattern analysis: (a) correlation function analysis, and (b) streak analysis to evaluate microfibril length.

beam stop and the equatorial streak. This operation is illustrated in Fig. 3(a).

A 1D Fourier transformation was then applied to it to obtain the correlation function

$$\gamma(x) = \frac{\int_0^\infty I_1(q_3)\cos(q_3 x)\, \mathrm{d}q_3}{\int_0^\infty I_1(q_3)\, \mathrm{d}q_3}. \quad (2)$$

By assuming a lamellar two-phase morphology, the long period, L, can be evaluated from the correlation function plot [32].

3.4.2. Lateral dimension of the fibril

In order to analyze the lateral dimension of the lamellar stack, a modified Guinier analysis [34,35] was adopted. For this analysis, the azimuthal profile of the lamellar reflection was first extracted. The lateral dimension, R, of the scattering entity, assumed to be rod like, can be obtained by the following equation:

$$\log I = \text{const} - \frac{q^2 R^2}{4 \times 2.303}, \quad (3)$$

where $q = 4\pi\sin\theta/\lambda$ is the scattering vector.

3.4.3. Fibril length

Analysis of the equatorial streak can be performed to extract the length of the microfibrils. This method was established by Grubb et al. [36].

As shown in Fig. 3(b), the lamellar reflections were first set to zero before longitudinal scans of the equatorial streak were taken perpendicular to the equator. These sliced profiles were fitted with Lorentzian functions. The integral breadths (IB) of these fitted peaks were found to increase with the scattering vector component q_{12} and can be fitted to the following equation [36]:

$$\frac{(\mathrm{IB})^2\cos(2\theta)}{\lambda D} = \frac{1}{2l_{\mathrm{f,v}}} + \left[\frac{1}{4l_{\mathrm{f,v}}} + \frac{q_{12}^2 \sin^2\beta_{\mathrm{f,v}}}{4\pi^2}\right]^{1/2}. \quad (4)$$

$q = 4\pi\sin\theta/\lambda$ is the scattering vector and q_{12} is its component in the equatorial direction, 2θ the scattering angle, λ the wavelength of the X-ray, D the sample-detector distance, $l_{\mathrm{f,v}}$ the length of the microfibril and $\beta_{\mathrm{f,v}}$ is the misorientation factor of the microfibril.

The length, $l_{\mathrm{f,v}}$ and the misorientation factor, $\beta_{\mathrm{f,v}}$, of the microfibril or microvoids can be obtained by a nonlinear fit of IB vs. q.

3.5. Optical birefringence

The optical birefringence measurements were made on POY prior to drawing at room temperature using a Carl Zeiss polarizing microscope with an Ehringhaus compensator (calcite plates). In order to obtain the optical birefringence, accurate measurements of the fiber diameter are necessary. These measurements were made directly using a Nikon optical microscope and a stage micrometer.

During the measurement of birefringence, the Ehringhaus compensator is carefully tilted until the color of the fiber center is compensated to black. The tilting angle of the Ehringhaus compensator corresponds to a phase difference, Γ (in units of nanometers). The optical birefringence Δn is given by

$$\Delta n = \frac{\Gamma}{d}, \quad (5)$$

where d is the diameter of the fiber in the unit of nanometers. It is to be mentioned that the orientation of the fiber is not uniform along the fiber, in that the color of the fiber under the polarized microscope is not the same. In this case, the color of the longest length in the sample is used to measure the birefringence.

4. Results and discussion

4.1. The effect of take-up speed on POY structure

Before presenting the drawing effect on fiber structure, it is useful to understand the structure dependence of undrawn POY on the take-up speeds. Off-line WAXD and SAXS were performed for POY prepared at different take-up speeds at room temperature. Three selected pairs of

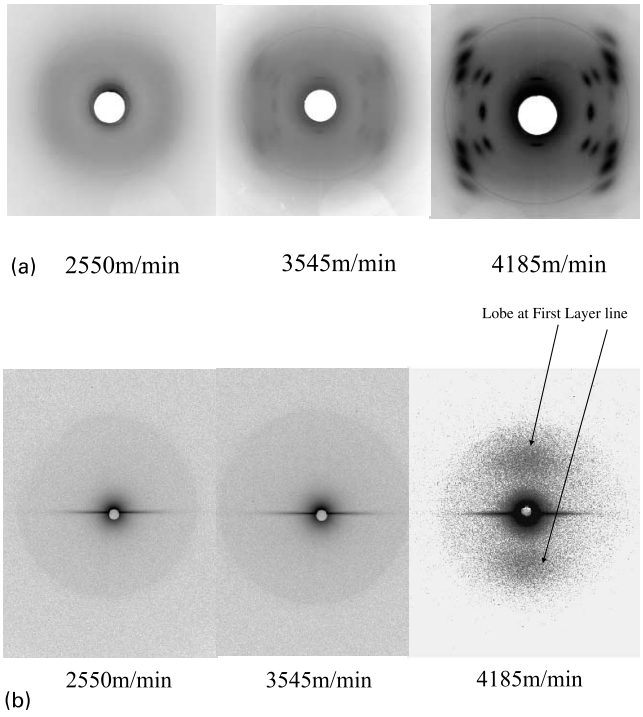

Fig. 4. Scattering patterns from POY prepared at 2550, 3545 and 4185 m/min. (a) WAXD patterns, and (b) SAXS patterns.

WAXD and SAXS patterns are shown in Fig. 4(a) and (b), respectively. The WAXS patterns for take-up speeds below some 3000 m/min (for example, the pattern for 2550 m/min) exhibit only broad intensity humps (amorphous scattering). The broad humps are more intense at the equator than at the meridian, signifying that the noncrystalline chains are oriented preferentially toward the fiber axis. The crystallinity dependence on take-up speed is shown in Fig. 5. For take-up speed below 3000 m/min, crystallinity is low and the error associated with the calculation is high. There is no substantial crystallinity development until the take-up speed is over 3000 m/min, which can be identified as the threshold for stress-induced crystallization. At 4185 m/min take-up speed, the crystallinity is about 18%. SAXS patterns for all take-up speeds exhibit a strong equatorial streak, indicating the presence of microfibrillar entities. The only SAXS pattern showing a pair of weak lobes on the meridian, suggesting the formation of lamellar stacks, is obtained from fiber of take-up speed of 4185 m/min, as shown in Fig. 4(b). The long period of the lamellar stack is 6.5 nm obtained using Eq. (2). Its lateral dimension is 2.5 nm using Eq. (3) and the length of microfibril is 15 nm using Eq. (4).

The birefringence results are shown in Fig. 6. Here one observes that the birefringence goes through a plateau before increasing again at about 3000 m/min. This result shows that the chain orientation is roughly the same for fibers prepared at take-up speeds between 1470 and 3000 m/min. Were the material homogeneous, the expectation would be that the chain orientation would increase monotonically with axial stress that is, with increasing take-up speed. But this is not observed. A suggested explanation is that a small concentration of very stiff, but noncrystalline, matter has been created and that this stiff material bears most of the axial load. Just such behavior has been noted by Janeschitz-Kriegl and Eder [37–41] for isotactic polypropylene under shear. In their work and that of others [42–44], the stiff, noncrystalline regions were shown to act as nucleation sites for subsequent crystallization. Further, McHugh and coworkers [42,43] (using high density polyethylene) and Kumaraswamy et al. [44] (using isotactic polypropylene) show that there is a critical melt strain for the creation of such oriented precursors. Likewise, the existence of an oriented amorphous phase in as-spun fibers of PET was established by Biangardi and Zachmann [45]. It was also shown [46] that it is the oriented amorphous phase that transforms into crystal during the heat treatment of PET. And Shimizu et al. have demonstrated that in PET fibers an oriented mesophase forms and increases in quantity over a take-up speed range of 2000–4000 m/min [47]. The existence of the birefringence plateau thus suggests (but certainly does not prove) that a rigid amorphous phase forms at take-up speeds in the range 980–3000 m/min, the lower limit corresponding to a critical

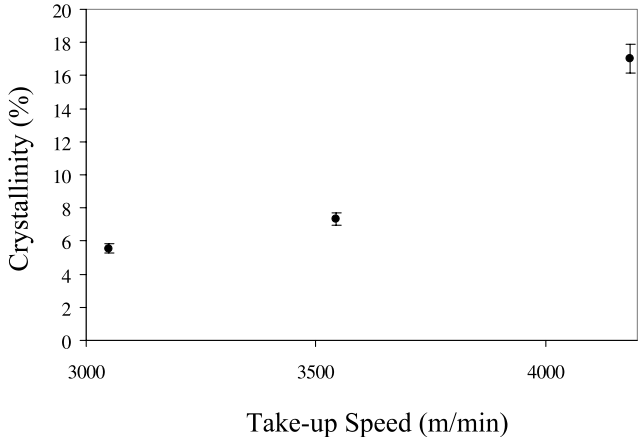

Fig. 5. Crystallinity vs. take-up speed for undrawn POY.

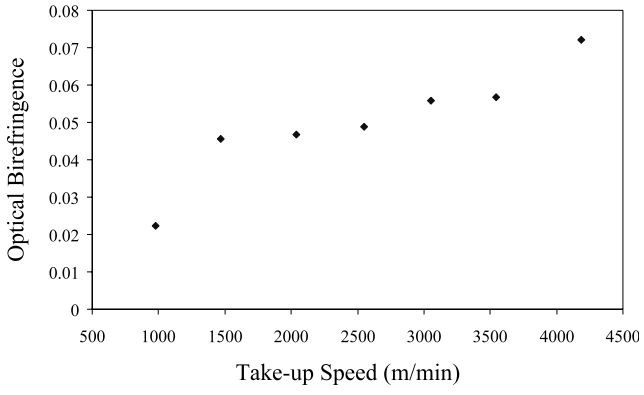

Fig. 6. Optical birefringence vs. take-up speed for undrawn POY.

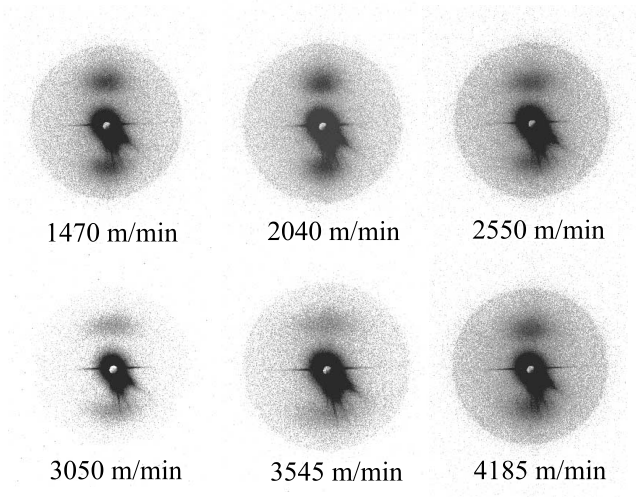

Fig. 7. SAXS patterns for POY of different take-up speeds drawn at 130°C and draw ratio of 1:1.

strain in the melt. It is further compelling to associate the suggested rigid amorphous material with the microfibrillar entities which are manifest as the equatorial SAXS streak. On this model, folded-chain crystals would grow laterally, using the suggested oriented microfibrils as nucleation sites. Stacks of such folded-chain crystals give rise to the meridinal SAXS peak.

4.2. The effect of drawing at 130°C and draw ratio 1:1

At 130°C, the drawing is not stable for draw ratios above 1.5:1. The draw ratio which gives the most stable drawing is 1:1 (constant length annealing). The SAXS and WAXD patterns taken for POY for take-up speeds from 1470 to 4185 m/min at this condition are shown in Figs. 7 and 8, respectively. The WAXD patterns show clearly that crystallinity develops at 130°C in fibers regardless of take-up speed. All SAXS patterns bearing a common

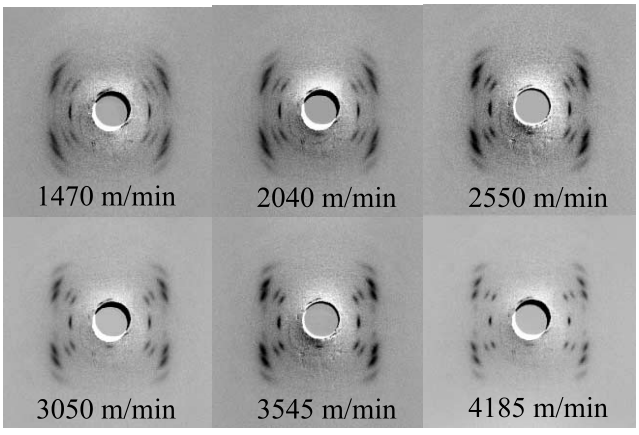

Fig. 8. WAXD patterns for POY of different take-up speeds drawn at 130°C and draw ratio of 1:1.

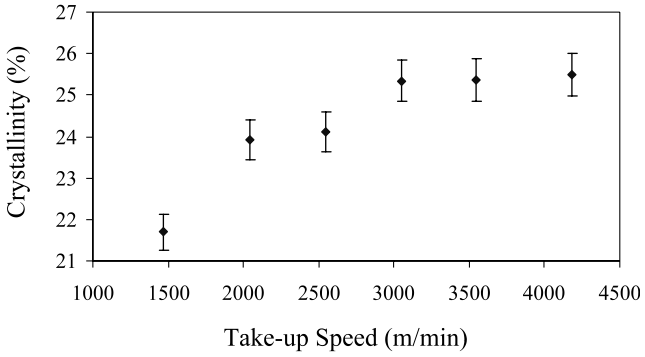

Fig. 9. Crystallinity dependence on preparation take-up speeds for POY drawn at 130°C and draw ratio of 1:1.

two-lobe feature suggest the formation of lamellar morphology in fiber of each take-up speed.

4.2.1. Crystallinity and orientation obtained from WAXD patterns

Fig. 9 shows that the crystallinity only slightly increases with take-up speeds when fiber are drawn at 130°C with draw ratio 1:1. This suggests that crystallinity for fiber drawn at 130°C is controlled by temperature instead of prior spinning history. Similarly, the orientation of crystals varies little with spinning take-up speed, as shown in Fig. 10.

4.2.2. Morphology suggested by SAXS patterns

The equatorial streak and lamellar lobe are common features of SAXS patterns in Fig. 7. The long period of the lamellar stacks and the length of the microfibrils, determined using Eqs. (2) and (4), are presented in Figs. 11 and 12, respectively.

With increasing take-up speed, the degree of chain extension increases. This results in the observed gradual increase in long period. The long period converges to about 7.7 nm at higher take-up speed. This value is characteristic of the PTT fiber system [6]. Correspondingly, the length of the microfibrils increases with increasing take-up speed, as shown in Fig. 12.

Looking further at Fig. 7, one finds that the shape of the SAXS scattering lobes transforms from lobe-like to arc-like as take-up speed increases from 1470 to 3545 m/min. This implies that the orientation of the lamellar stacks decreases

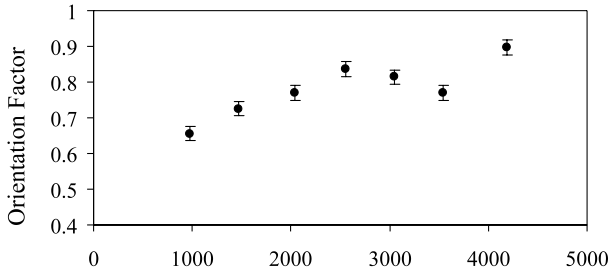

Fig. 10. Orientation factor dependence on preparation take-up speeds for POY drawn at 130°C and draw ratio of 1:1.

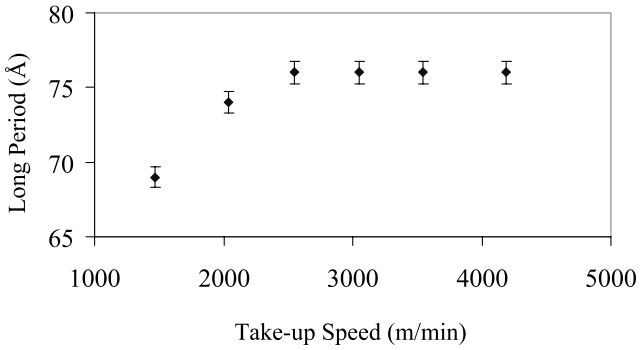

Fig. 11. Dependence of long period of lamellar structure on preparation take-up speeds for POY drawn at 130°C and draw ratio of 1:1.

with increasing take-up speed in this range. Over this same take-up speed range, the chain axes within the crystals increases slightly (Fig. 10), except perhaps near the end of the range. We offer no explanation for this phenomenon.

For fibers of 4185 m/min, the lamellar morphology pre-exists in the as-spun fibers, which is also observed during drawing. Using Eqs. (2)–(4), the long period, lateral dimension of the lamellar stacks and the microfibril length of the drawn fiber are evaluated and compared to the undrawn values. They increase from 6.5 to 7.7, 2.5 to 3.9 and from 15 to 22 nm, respectively. Therefore, at temperature 130°C with little line tension, crystals have grown both axially and transversely relative to the microfibrils which are formed during spinning at a take-up speed of 4185 m/min.

4.3. Drawing at 100°C

At this temperature, the drawing is relatively stable. Fibers prepared at take-up speeds of 980, 2550 and 4185 m/min, can be drawn up to a draw ratio of 3:1. The resulting SAXS patterns, which are not shown, are similar to those obtained at 130°C, showing a two-lobe feature and an equatorial streak. The WAXD patterns are shown in Fig. 13(a)–(c). Looking through the three parts of Fig. 13, one observes that the orientation of crystallites increases with draw ratio, as expected. A calculation of the orientation

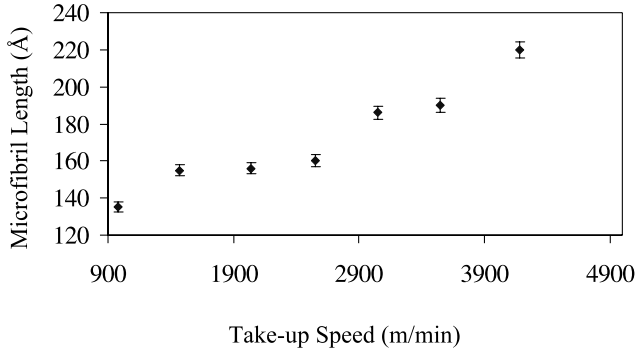

Fig. 12. Dependence of microfibril length on preparation take-up speeds for POY drawn at 130°C and draw ratio of 1:1.

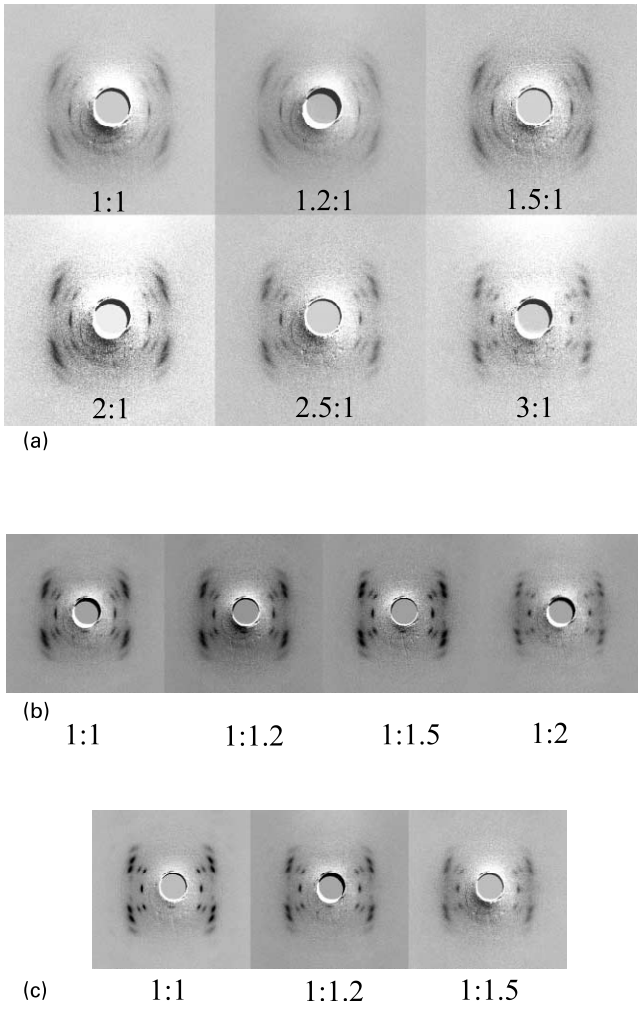

Fig. 13. WAXD patterns for POY drawn at 100°C and at different draw ratios: (a) take-up speed = 980 m/min, (b) take-up speed = 2550 m/min, and (c) take-up speed = 4185 m/min. The draw ratio is marked on each pattern.

factor is done for fiber of take-up speed of 980 m/min and is shown in Fig. 14.

4.3.1. Crystallinity and unit cell dimensions obtained from WAXD patterns

The crystallinity dependence on draw ratio for fiber of take-up speeds 980, 2550, 4185 m/min at 100°C is shown in Fig. 15. For fibers prepared at different take-up speeds, the dependence is quite different. For the case of 4185 m/min, a monotonic decrease is observed. For the case of 2550 m/min, crystallinity stays nearly constant, while for that of 980 m/min, crystallinity first goes through a maximum before decreasing with increasing draw ratio.

The dependence of the a, b, c dimensions of the unit cell on draw ratio has also been extracted from WAXD patterns and is shown in (a)–(c) parts of Fig. 16. For fiber of 980 m/min, the unit cell dimensions a, b, c remain nearly constant. For fibers of 4185 m/min, a substantial increase in c and a slight increase in a and b are

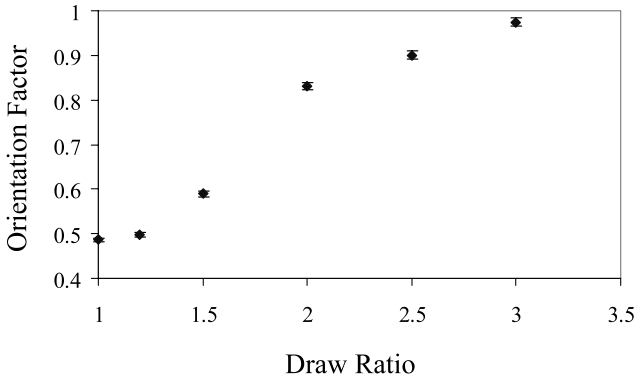

Fig. 14. Orientation factor dependence of POY of take-up speed 980°C and drawn at 100°C on draw ratios.

observed. For fibers of 2550 m/min, the *c* dimension stays nearly constant for draw ratios up to 1.5 and a sudden increase is observed at draw ratio of 2, while the *a* and *b* dimensions remain nearly constant with a slight trend of increase.

Similar to the situation at 130°C, the crystallinity, which is about 20%, is temperature-controlled and does not depend on the prior spinning history at 100°C when the draw ratio is 1:1. For fiber spun at 4185 m/min, the as-spun crystallinity is about 18%, as shown in Fig. 5, while little crystallinity exists in as-spun fibers whose take-up speed is 980 or 2550 m/min. Therefore, the effect of drawing would be to modify the crystals formed during spinning when the take-up speed is 4185 m/min, while drawing induces crystallization and rearranges the induced crystals for the other two cases.

Let us consider the drawing of fiber of 4185 m/min first. In this case, the *c* dimension increases significantly, from 19.5 to 23 Å. In the crystal structure described in Section 1, the chains are in a helical *trans–gauche–gauche–trans* (*tggt*) conformation, as modeled in the lower part of Fig. 17. In this case, the repeat distance is 1.86 nm. Were the chains to straighten themselves, taking an all-*trans* (*tttt*) conformation, as in the upper part of Fig. 17, the repeat distance would be 2.36 nm. (An independent simulation [49] also concludes that an all-*trans* PTT unit cell should posses a *c* dimension of 2.36 nm.) These values suggest that

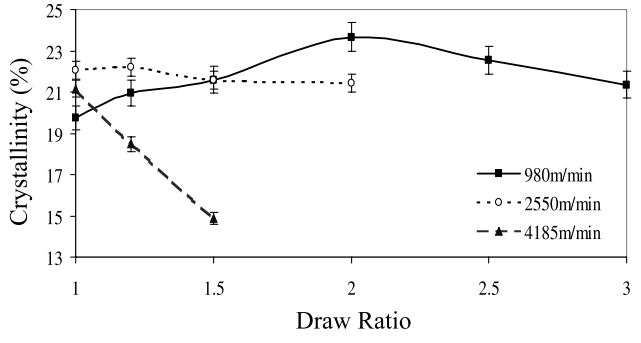

Fig. 15. Crystallinity dependence of POY drawn at 100°C on draw ratios.

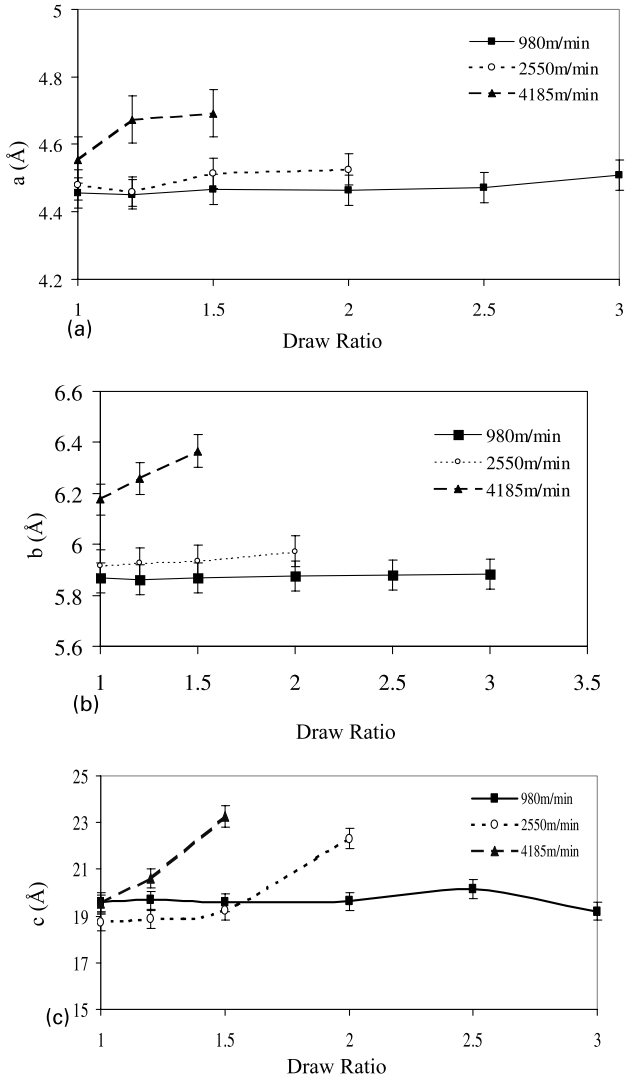

Fig. 16. Dependence of unit cell dimensions of unit cell of POY drawn at 100°C on draw ratios. (a) *a* dimension, (b) *b* dimension, and (c) *c* dimension.

the crystals undergo a gradual conformational transformation upon drawing at 100°C, from *tggt* to *tttt*. It is, however, topologically impossible for all of the chains in a crystallite to simultaneously undergo the complete rotations associated with such conformational chains. It is more likely that the conformational transition is implemented by the creation and transport of conformational defects along the chains, facilitated by internal rotation of the chains [48]. In order to maintain the continuity of the crystal, defects would have to be created and transported in all chains at about the same time. Due to this existence of large concentration of conformational defects in the crystals, the *a* and *b* dimensions of the crystals are expected to increase. Also, crystals would appear to be 'melting' locally, due to the existence of defects, and an apparent decrease in crystallinity is expected. Indeed, the expected qualitative trends in *a* and *b* dimensions and crystallinity are observed. Note, however, that no deviations of unit cell dimensions from the equilibrium values are observed for fibers spun at 4185 m/min and

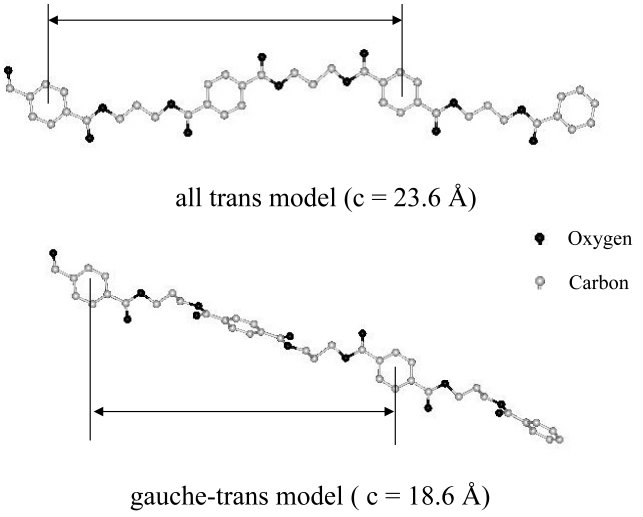

Fig. 17. Simulation of *c* dimension of the unit cell of PTT for all-*trans* and all-*gauche* configuration.

drawing at 130°C at a draw ratio of 1:1. This suggests that drawing stress is important in activating the process, perhaps facilitating the formation of conformational defects. High temperature alone, 100 or 130°C, produces only crystal growth. Similar phenomena have been observed in polyolefins or substituted polyolefins such as polypropylene, polyethylene and poly(tetrafluoroethylene) [48].

For the case of take-up speeds 2550 m/min, crystallinity stays relatively constant, except for the highest draw ratio of 2:1, at which point a slight decrease is observed. Correspondingly, an increase in the *c* dimension can be observed at the same draw ratio. Assuming that the crystals induced during drawing are much less defective than those formed during spinning, then the explanation for the case of 4185 m/min can also be applied here, except only that a higher draw-line stress, corresponding to a draw ratio of 2:1, is necessary to activate the transition. Similarly, the same explanation can be applied to the 980 m/min fibers. For this case, an initial draw ratio up to 2:1 still induces crystallization, while the *c* dimension is relatively constant through out all draw ratios.

4.3.2. Lamellar morphology at 100°C

At this stage, it is useful to visit the long period extracted from SAXS patterns, as shown in Fig. 18, to understand to the rigid amorphous phase behavior in PTT fibers. For the fibers prepared at take-up speeds of 4185 and 2550 m/min, the long period increases with draw ratio. The numerical value can be correlated well with the increase in the *c* dimension of the unit cell. It appears that the rigid amorphous phase for these fibers is incapable of extension and it is the change in *c* dimension of the unit cell that is responsible for the long period increase.

For the case of fiber of 980 m/min, the long period initially decreases with increasing strain, before exhibiting a minimum. For these fibers the unit cell dimension stays

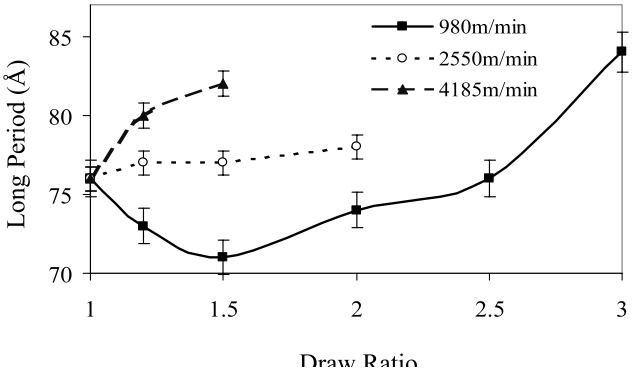

Fig. 18. Dependence of long period of POY drawn at 100°C on draw ratios.

relatively constant with strain, while crystallinity increases. It is likely the growth of more dense crystals into the less dense amorphous layer that is responsible for the initial decrease in long period. When the draw ratio is above 1.5:1, the high external stress begins to extend coiled amorphous chains and this leads to an increase in the long period.

4.4. Temperature effects

Presented in Fig. 19 is the effect of temperature on fibers of 980, 2550, 4185 m/min at a draw ratio of 1:1. The corresponding crystallinity is also marked on each pattern.

For fibers of 980 and 2550 m/min take-up speeds, increasing temperature results in an increase in crystallinity. Again, the crystallinity is likely a transformation from the oriented amorphous phase. For fibers of 4185 m/min take-up speed, due to the preexistence of crystallinity in the as-spun fiber, as shown in Fig. 5, crystallinity is not sensitive to temperature increase to 100°C. At 130°C, additional crystallization has been induced.

It is necessary to point out that there is no development of

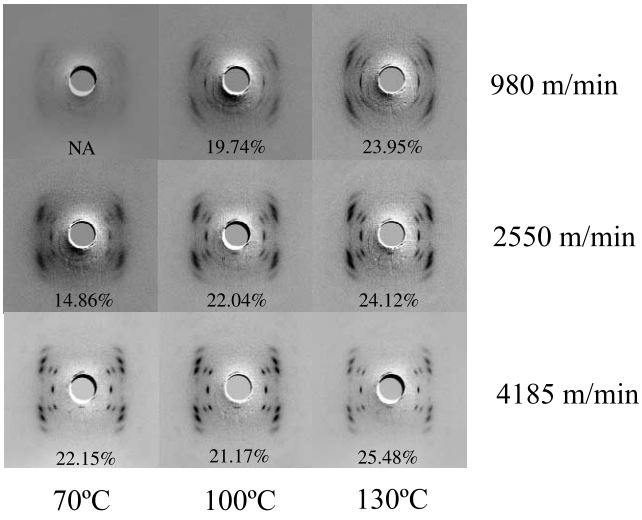

Fig. 19. WAXD patterns illustrating of temperature effect on fiber crystallinity. The crystallinity is marked on each pattern.

lamellar structure at 70°C for as-spun fibers, as suggested by the SAXS patterns lacking the two-lobe feature.

5. Conclusions

Both SWAXS and birefringence off-line measurements on PTT POY suggest the formation of a rigid amorphous phase during spinning, and this affects the structure and morphology of these fibers upon further hot-drawing. At temperatures above 100°C and draw ratio 1:1, the crystallinity is temperature-controlled and is independent of prior spinning history. The corresponding SAXS pattern shows the formation of lamellar stacks. The lateral growth of crystallites with extended chains as nucleation sites is suggested. At temperatures above 100°C and draw ratios above 1:1, the crystal structure is a function of both draw ratio and prior take-up speed. For fibers prepared at 4185 m/min, the draw-line stress plays an important role in concurrent defect creation and transport in all chains. This leads to the gradual transformation of chain conformation from *tggt* to *tttt*, with an increase in the *c* dimension of the unit cell and a concomitant decrease in crystallinity with drawing. For fibers prepared at lower take-up speeds, a mixed process of crystallization and defect creation/transport is suggested.

Acknowledgements

JW and JMS gratefully acknowledge the financial support by NSF GOALI grant DMR-9629825.

References

[1] Desborough IJ, Hall IH, Neisser JZ. Polymer 1979;20:545.
[2] Dandurand SP, Perez S, Revol JF, Brisse F. Polymer 1979;20:419.
[3] Hall IH. In: Hall IH, editor. Structure of crystalline polymers. Amsterdam: Elsevier, 1984. p. 58.
[4] Hall IH. In: Hall IH, editor. Structure of crystalline polymers. Amsterdam: Elsevier, 1984. p. 39.
[5] Jakeways R, Ward IM, Wilding MA, Hall IH. J Polym Sci, Polym Phys Ed 1975;13:799.
[6] Ward IM, Wilding MA, Brody H. J Polym Sci, Polym Phys Ed 1976;14:263.
[7] Katayama K, Amano T, Nakamura K. Kolloid Z Z Polym 1968;226:125.
[8] Spruiell J, White J. Polym Engng Sci 1975;15:660.
[9] Haberkorn H, Hahn K, Breuer K. J Appl Polym Sci 1993;47:1551.
[10] Hsiao BS, Kennedy AD, Leach RA, Chu B, Harney P. J Appl Cryst 1997;30:1084.
[11] Smith FS, Steward RD. Polymer 1974;15:283.
[12] Alfonso GC, Verdona MP, Wasiak A. Polymer 1978;19:711.
[13] Althen G, Zachmann HG. Makromol Chem 1979;180:2723.
[14] Kobayashi K, Nagasawa T. J Macromol Sci Phys 1970;B4:331.
[15] Price FP. In: Zettelmoyer AC, editor. Nucleation. New York: Marcel Dekker, 1969.
[16] McHugh AJ, Forrest EH. J Macromol Sci Phys 1975;B11:219.
[17] Yeh GSY, Hong KZ. Polym Engng Sci 1979;19:395.
[18] Dismore PD, Statton WO. J Polym Sci 1964;B2:1113.
[19] Dismore PD, Statton WO. J Polym Sci A-2 1966;7:113.
[20] Dumbleton JH. J Polym Sci A-2 1969;7:667.
[21] Liska E. Kolloid Z 1973;251:1029.
[22] Bonart R. Kolloid Z 1973;231:438.
[23] Fisher EW, Fakirov S. J Mater Sci 1976;11:1041.
[24] Gupte KM, Motz H, Schultz JM. J Polym Sci, Polym Phys Ed 1983;21:1927.
[25] Wu J, Schultz JM, Samon JM, Pangelinan AB, Chuah HH. Polymer 2001;42:7131.
[26] BaltaCalleja FJ, Vonk CG. X-ray scattering of synthetic polymers. Amsterdam: Elsevier, 1989.
[27] Hermans PH, Platzek P. Kolloid Z 1939;88:68.
[28] Hermans PH, DeBooys JJ. Kolloid Z 1939;88:73.
[29] Hermans PH, Hermans JJ, Vermaas D, Weidinger AJ. J Polym Sci 1947;3:1.
[30] Alexander LE. X-ray diffraction methods in polymer science. New York: Wiley, 1969.
[31] Wilchinsky ZW. J Appl Phys 1960;31:1969.
[32] Bonart R, Hosemann R. Kolloid Z Z Polymer 1962;186:16.
[33] Strobl GR, Schneider M. J Polym Sci, Part B: Polym Phys 1980;18:1343.
[34] Guinier A, Fournet G. Small-angle scattering of X-rays. New York: Wiley, 1955.
[35] Murthy NS, Bednarcayk C, Moore RAF, Grubb DT. J Appl Polym Sci: Part B: Polym Phys 1996;34:821–35.
[36] Grubb DT, Prasad K. Macromolecules 1992;25:4575.
[37] Janeschitz-Kriegl H, Wimberger-Friedl R, Krobath G, Liedauer S. Kunststoffe 1987;40:301.
[38] Eder G, Janeschitz-Kriegl H. Colloid Polym Sci 1988;266:1087.
[39] Eder G, Janeschitz-Kriegl H, Krobath G. Prog Colloid Polym Sci 1989;80:1.
[40] Eder G, Janeschitz-Kriegl H, Liedauer S. Prog Polym Sci 1990;15:629.
[41] Jerschow P, Janeschitz-Kriegl H. Int Polym Processing 1997;12:72.
[42] McHugh AJ, Guy RK, Tree DA. Colloid Polym Sci 1993;271:629.
[43] Bushman AC, McHugh AJ. J Appl Polym Sci 1997;64:2165.
[44] Kumaraswamy G, Issaian AM, Kornfield JA. Macromolecules 1999;32:7537.
[45] Biangardi HJ, Zachmann HG. Makromol Chem 1976;177:1173.
[46] Ziabicki A, Jarecki L. Colloid Polym Sci 1978;256:332.
[47] Shimizu J, Kikutani T, Takaku A. In: Proceedings of the International Symposium on Fiber Science and Technology, ISF-85, August 1985. Essex, UK: Elsevier; 1986. p. 2.
[48] Rastogi S, Newman M, Keller A, Hikosaka M. In: Dosiere M, editor. Crystallization of polymers, NATO ASI Series, vol. 451. Dordrecht, The Netherlands: Kluwer Academic Publishers, 1993.
[49] Iannelli P, private communication.